CRYSTAL STRUCTURE OF POLYMORPH II AND PRESSURE-TEMPERATURE PHASE DIAGRAM OF THE DIMORPHIC ANAESTHETIC BUTAMBEN

Ivo B. Rietveld[1, 2]*, Maria Barrio[3], René Ceolin[3], Josep-Lluis Tamarit[3]

[1] Normandie Université, Laboratoire SMS - EA 3233, Université de Rouen, F 76821 Mont Saint Aignan, France
[2] Faculté de Pharmacie, Université de Paris, 4 avenue de l'observatoire, 75006, Paris, France
[3] Grup de Caracterització de Materials, Departament de Física and Barcelona Research Center in Multiscale Science and Engineering, Universitat Politècnica de Catalunya, EEBE, Campus Diagonal-Besòs, Av. Eduard Maristany 10-14, 08019 Barcelona, Catalunya, Spain

* Corresponding author: ivo.rietveld@univ-rouen.fr. Current address:
Neutron Science Laboratory, Institute for Solid State Physics, University of Tokyo, 5-1-5 Kashiwanoha, Kashiwa, Chiba 277-8581, Japan.

Abstract

The crystal structure of the low-temperature form II of butamben has been solved in a $P2_1/c$ space group very similar to that of form I. Form II possesses virtually the same packing as that of the high-temperature form I and the dimorphism is mainly represented by a small discontinuous change in the size of the unit cell and in its enthalpy. Due to the small enthalpy difference between the two polymorphs of 375 $J \cdot mol^{-1}$, it will be difficult to predict the change in the stability hierarchy by computer-aided methods. The pressure-temperature phase diagram, constructed using volume and enthalpy differences between the two phases at ordinary pressure, corresponds to a case of overall enantiotropy, as the I-II and I-L equilibrium lines diverge with increasing pressure. This conclusion is confirmed by the experimental pressure-temperature phase diagram obtained with differential thermal analysis measurements under pressure.

Keywords
Butamben, dimorphism, crystallographic properties, thermodynamic properties, pressure-temperature phase diagram, crystal structure

1 Introduction

1.1 Butamben

Butamben, *p*-aminobenzoic acid butyl ester, or butyl 4-aminobenzoate, is a local anaesthetic whose formula is provided in **Figure 1**.

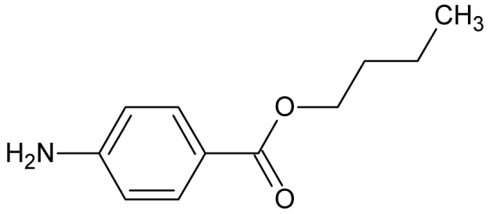

Figure 1. Molecular structure of butamben $C_{11}H_{15}NO_2$ with M = 193.24 g·mol^{-1}

Together with benzocaine and isobutamben, butamben belongs to a series of esters of p-aminobenzoic acid with anaesthetic properties that have been found to exhibit crystalline polymorphism.[1] In a previous article, the pressure-temperature (P-T) phase diagram involving forms II and III of benzocaine was investigated[2] resulting in a case of enantiotropy turning to monotropy on increasing the pressure similar to the paradigmatic case of the sulphur P-T phase diagram, or the first case of the four cases formerly described and drawn by Bakhuis Roozeboom.[3-5]
As part of a study into the polymorphism of these esters and out of a more general interest into the comparison between topological and experimental P-T phase diagrams, the construction of the P-T phase diagram of the dimorphism of butamben is reported in the present article together with the crystal structure of the low-temperature polymorph.

1.2 Available data from the literature

The room temperature structure of butamben was recognized to be monoclinic by Watanabe in 2002 and solved in 2004 by Caira et al.[6,7] The latter found a monoclinic $P2_1/c$ structure with parameters a = 8.3508(5) Å, b = 5.2093(4) Å, c = 25.626(2) Å, β = 95.372(2)°, and a density of 1.156 g·cm^{-3} at 298(2) K.[7] The CIF of the structure is available in the Cambridge Structural Database (CSD) under the reference EZAVIK.
According to Schmidt,[1] the commercial powder of this monoclinic butamben (form I) melts at 330.5 K (onset) with a melting enthalpy of 23.9 kJ·mol^{-1} (123.68 J·g^{-1}). In addition, this author reported that on cooling the commercial sample at a rate of 5 K·min^{-1}, a phase transition to another form, thus named form II, was observed. On heating, the form II to form I transition was found to occur at 285.1 K (onset) with an enthalpy of 0.8 kJ·mol^{-1} (4.16 J·g^{-1}).
Recently, the dimorphism of butamben was reinvestigated by Svärd et al.[8] They reported the X-ray powder diffraction profile of form II in addition to melting data near those previously found: $T_{I\rightarrow L}$ = 330.56 K (L = liquid), $\Delta_{I\rightarrow L}H$ = 24.7 kJ·mol^{-1} (127.82 J·g^{-1}), while the transition enthalpy at $T_{II\rightarrow I}$ = 282.93 K was reported to be $\Delta_{II\rightarrow I}H$ = 0.39 kJ·mol^{-1} (2.02 J·g^{-1}), i.e. twice as small as that reported by Schmidt.[1] In addition Svärd et al. determined the temperature dependence of the specific heats of form I and of the melt in the form Cp /J·mol^{-1}·K^{-1} = k_1T /K + k_2 with $k_{1,I}$ = 1.2399 J·mol^{-1}·K^{-2}, $k_{2,I}$ = -57.7 J·mol^{-1}·K^{-1} and $k_{1,L}$ = 0.3752 J·mol^{-1}·K^{-2} and $k_{2,L}$ = 257.4 J·mol^{-1}·K^{-1}.[8]

2 Experimental

2.1 Materials

Butamben (purity ≥ 98%) was purchased from Fluka and used as such.

2.2 Differential Scanning Calorimetry (DSC)

Temperatures (onset) and heats of transition have been obtained with a Q100 thermal analyser from TA Instruments at various rates. The analyser was calibrated using the melting point of indium (T_{fus} = 429.75 K and $\Delta_{fus}H$ = 28.45 J g^{-1}). Butamben specimens were weighed using a microbalance sensitive to 0.01 mg and sealed in aluminium pans.

2.3 Densitometry of the melt as a function of temperature

Liquid density as a function of temperature was measured with a DMA-5000 Density Meter from Anton-Paar. A melted specimen was introduced in the apparatus equilibrated at a temperature above the temperature of fusion. Data were obtained at isothermal steps while slowly cooling in the temperature range from 363 to 323 K. Dry air and bi-distilled water were used as calibration standards in the temperature range. The temperature was controlled at ±1 mK and measurements were performed when temperature fluctuations were smaller than ± 0.5 mK.

2.4 High-resolution X-ray powder diffraction

XRPD measurements were performed with a vertically mounted INEL (Artenay, France) cylindrical position-sensitive detector (CPS-120) using the Debye–Scherrer geometry and transmission mode (angular step 0.029° over a 2θ-range of 2 to 112°). Monochromatic Cu-Kα_1 (λ = 1.54056 Å) radiation (35 kV, 35 mA) was selected by means of a focusing incident-beam germanium monochromator. Measurements as a function of temperature were carried out using a liquid nitrogen 700 series Cryostream Cooler from Oxford Cryosystems. Cubic $Na_2Ca_3Al_2F_4$ was used for external calibration. The PEAKOC application from DIFFRACTINEL software was used for the calibration as well as for the peak position determinations after pseudo-Voigt fittings and lattice parameters were refined by way of the least-squares option of the FullProf suite.[9,10]
Butamben samples were introduced in a Lindemann capillary (0.5-mm diameter). The capillaries were rotated perpendicularly to the X-ray beam during the experiments to improve the averaging of the crystallite orientations. Before each isothermal data acquisition, the samples were allowed to equilibrate for about 10 min, and each acquisition time was no less than 1 h. The heating rate in-between data collection was 1.33 K min^{-1}. Patterns were recorded on heating in the temperature range from 100 K up to the melting point.

2.5 High-pressure differential thermal analysis (HP-DTA)

HP-DTA measurements have been carried out at constant applied pressure with two differential thermal analyzers. For the temperature of fusion, an in-house constructed apparatus similar to that designed by Würflinger was used.[11] The copper-beryllium

Bridgman pressure cell allows pressures up to 300 MPa and temperatures up to 393 K. It uses chromel-alumel thermocouples as thermal sensors. The sensitivity of the latter does not allow to detect low energy signals; therefore, for the II-I transition measurements, an MV1-30 high-pressure cell was used, developed at the Institute of High Pressure Physics (Polish Academy of Science), with Peltier elements as thermal sensors.[12] In both devices, a similar pressure range was scanned and the measurements were carried out at the same heating rate of 2 K min^{-1}. To determine the melting temperature as a function of pressure and to ascertain that in-pan volumes were free from residual air, specimens were mixed with an inert perfluorinated liquid (Galden®, from Bioblock Scientifics, Illkirch, France) as a pressure-transmitting medium, and the mixtures were sealed into cylindrical tin pans. To verify that the perfluorinated liquid was chemically inactive and did not interfere with the melting temperature of butamben, preliminary DSC measurements were carried out with a Galden®-butamben mixture on the Q100 analyser of TA instruments without applied pressure.

2.6 Structure Solution from Powder Diffraction

For the structure solution of the low temperature form II, 24 hours of diffraction intensity was accumulated at 120 K. The program DASH 3.4.5 was employed and the powder pattern was truncated from 6.12 to 55.5◦ in 2θ (λ-Cu-Kα_1), corresponding to a real space resolution of 1.65 Å. The background was subtracted with a Bayesian high-pass filter. Twenty peak positions for indexing were obtained by fitting with an asymmetry-corrected pseudo-Voigt function.[13,14] They were indexed with the program DICVOL91.[15] A monoclinic unit cell was obtained. The figures of merit given by DICVOL were $M(20)$ = 11.4 and $F(20)$ = 18.3 (0.0176, 62). Although these values were relatively low, the unit cell was selected due to its similarity with the high temperature phase. Pawley refinement was used to extract integrated intensities and their correlations, from which the space group was determined using Bayesian statistical analysis.[16] The extinction symbol C1-1 had the highest probability directly followed by $P2_1/a$. Despite the high probability, it was not possible to fit the pattern against space group C2 as several reflections violate the extinction rules for this space group. The high temperature form of butamben has space group $P2_1/c$,[7] so $P2_1/c$ while inverting the a and c axes of the unit cell was chosen for further investigation. It resulted in a Pawley χ^2 of 6.154. Simulated annealing was used to solve the crystal structure from the powder pattern in direct space. The starting molecular geometry was taken from the published room temperature form from the Cambridge Structural Database (reference code EZAVIK).[7] In 30 simulated annealing runs, the same crystal structure was found 30 times. The profile χ^2 of the best solution was 25.89, which is four times the Pawley χ^2; this is a good indication that the correct solution has been found.

For the Rietveld refinement, data up to 64° 2θ were used, which corresponds to 1.45 Å real-space resolution. The Rietveld refinement was carried out with TOPAS-Academic.[17] Bond lengths, bond angles, and planar groups were subjected to suitable restraints, including bonds to H atoms. A global Biso (isotropic temperature parameter) was refined for all non-hydrogen atoms, with the Biso of the hydrogen atoms constrained at 1.2 times the value of the global Biso. The inclusion of a preferred-orientation correction with the March-Dollase formula was tried for directions (100), (010), and (001).[18] None of the directions made a significant difference to the Rwp value (coefficient for comparison between measured and calculated powder pattern). The molecular geometry was checked with Mogul, which compares each bond length and bond angle with

corresponding distributions from single-crystal data.[19] No unusual bond lengths, angles, torsion angles or rings were found.
Supplementary crystallographic data can be found in the CCDC, deposit number 2087260, and obtained free of charge from the Cambridge Crystallographic Data Centre via www.ccdc.cam.ac.uk/data request/cif/.

3 Results

3.1 Crystal structure of the low-temperature form II

The Rietveld refinement progressed smoothly and produced a good fit with χ^2 = 1.724, R'p = 14.706, R'wp = 14.834 (values after background correction), Rp = 4.587, and Rwp = 6.405 (values before background subtraction). Biso refined to 0.2(2) Å^2. Crystal data and the details of the structure refinement have been compiled in the Supporting information **Table S1**. The structure was found to be monoclinic, space group $P2_1/c$ (Z = 4), with cell parameters a = 8.2634(5) Å, b = 4.7330(2) Å, c = 27.626(2) Å, β = 95.604(5)° and a unit-cell volume of 1075.3(1) Å^3. The result of the Rietveld refinement is shown in **Figure 2** and the unit-cell in **Figure 3**. The molecular structure with the same atom labels as in the cif EZAVIK, form I, can be found in the **Supporting information Figure S1.** The atom coordinates have been compiled in the **Supporting information Table S2** and a full powder X-ray diffraction pattern obtained for this polymorph is available in the **Supporting information Figure S2**.

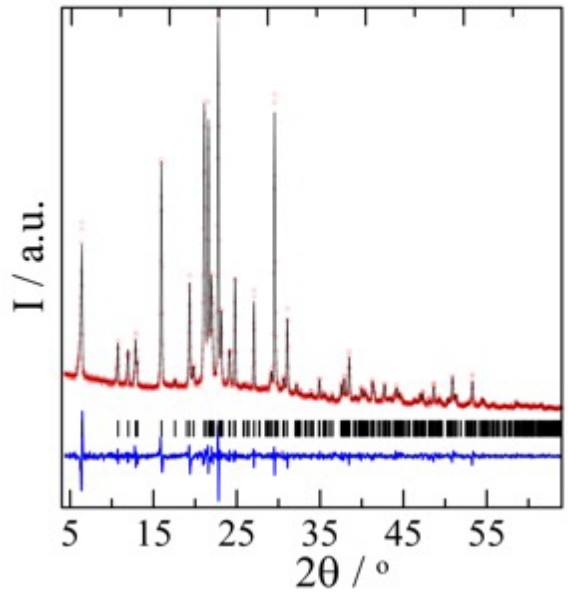

Figure 2. Rietveld refinement of butamben form II at 120 K. Experimental (red) and calculated (black) profiles, and obs-calc difference (blue) with peak positions (vertical segments in black).

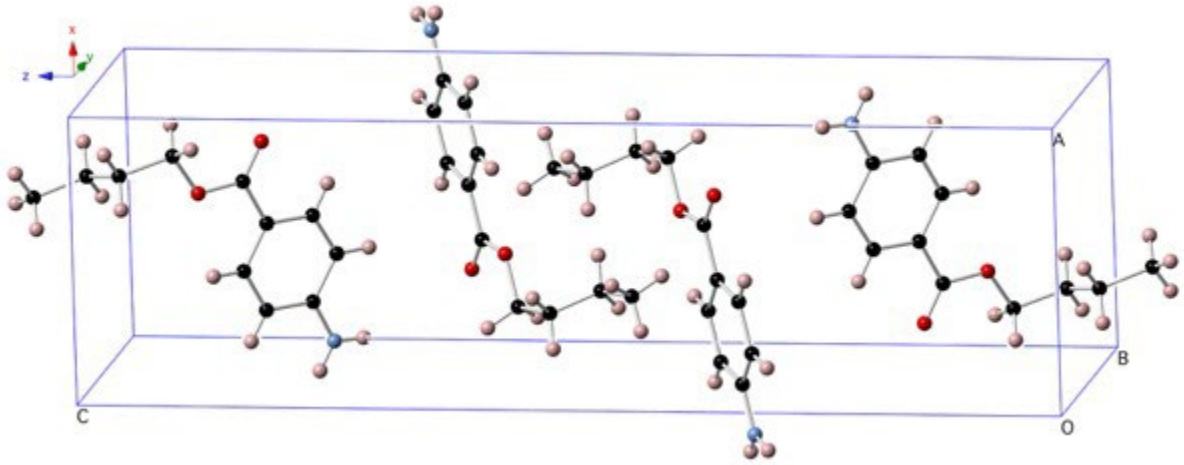

Figure 3. Unit-cell of the low-temperature form II of butamben at 120 K with the following atom colour coding: O = red, N = blue, C = black, H = pink.

3.2 Calorimetric data of the phase equilibria

The onset temperatures and heats of transition for the phase transitions II→I and I→L from several runs at various heating rates have been compiled in **Table S3**, in which it can be seen that the enthalpy changes are virtually independent of the heating rate. Thus, the mean values have been determined with all the data points, leading to 1.94(50) $J \cdot g^{-1}$ (or 375 $J \cdot mol^{-1}$) for the II→I transition and 128.7(4.4) $J \cdot g^{-1}$ for the fusion of form I. On the other hand, it can be seen that the onset temperatures slightly depend on the heating rate, although this dependence vanishes for heating rates lower than 10 $K \cdot min^{-1}$ (**Figure 4**). Therefore, the mean onset temperatures were determined with values obtained at heating rates equal to and lower than 10 $K \cdot min^{-1}$ resulting in the following values: $T_{II \rightarrow I}$ = 282.9(2) K and $T_{I \rightarrow L}$ = 330.2(3) K.

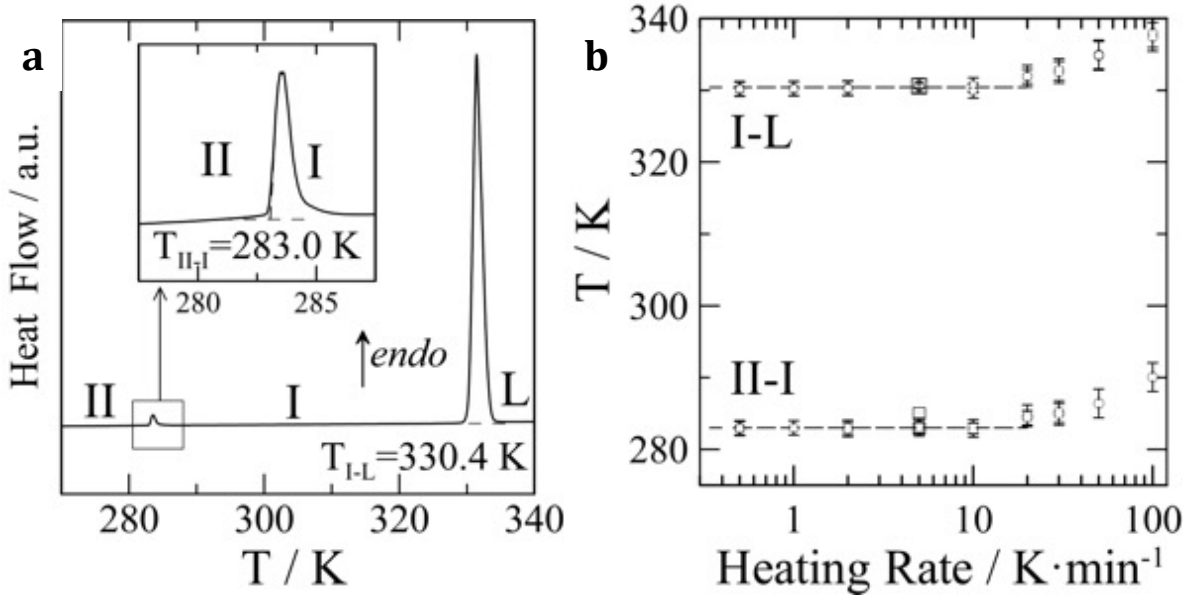

Figure 4. (a) Differential scanning calorimetry curve of butamben form II (m = 9.91 mg) heated at a 0.5 K min^{-1} rate and **(b)** dependence on the heating rate of the onset temperatures of the II-I and I-L transitions.

3.3 Specific volume as a function of temperature

Values of the specific volume of molten butamben as a function of temperature obtained with density measurements have been reported in the **Supporting information** Table S4. They have been fitted to the following equation:

v_{liq} /cm^3·g^{-1} = 0.7169(9) + 0.000720(3) T/K (r^2 = 0.99992) **(1)**

Lattice parameters and specific volumes of both forms, obtained from two series of high-resolution X-ray diffraction patterns at various temperatures (**Figure 5**), have been compiled in **Supporting information** Table S5. The dependence of the specific volumes of forms I and II on the temperature have been fitted to the following equations with v in cm^3·g^{-1} and T in K:

v_I = 0.790(7) + 2.69(22) ×10^{-4} T (r^2 = 0.93) **(2)**

v_{II} = 0.830(4) + 3.08(4.32) ×10^{-5} T + 3.4(1.1) ×10^{-7} T^2 (r^2 = 0.98) **(3)**

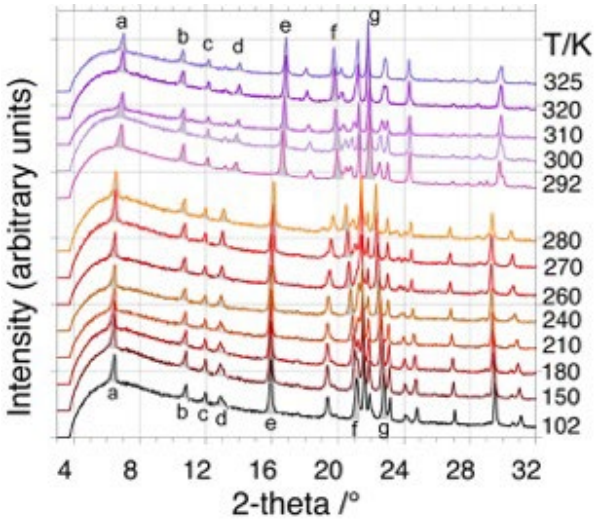

Figure 5. One series of high-resolution X-ray powder diffraction patterns of butamben polymorphs: low-temperature form II from 102 K to 280 K, high-temperature form I from 292 K to fusion. A number of peaks with the same Miller indices have been coloured in grey and identified by a letter: a = 0 0 2, b = 1 0 0, c = 1 0 -2, d = 0 0 4, e = 1 0 -4, f = 0 1 3, g = 1 0 4.

3.4 The phase equilibria under pressure

The onset temperatures of the II→I and I→L phase changes from at a number of different pressures up to 370 MPa are presented in **Figure 6**. It can be seen that the transition temperatures, for the solid-solid equilibrium as well as for the melting equilibrium, linearly depend on the pressure and the fitted equations are as follows:

$P_{I\text{-}II}$ /MPa = 9.24(33) T /K –2594(99) (r^2 = 0.991) **(4)**

$P_{I\text{-}L}$ /MPa = 7.02(17) T /K –2319(60) (r^2 = 0.980) **(5)**

The temperatures and pressures for the two equilibrium curves can be found in **Supporting information Table S6,** and the related HP-DTA peaks in **Supporting information Figure S4**.

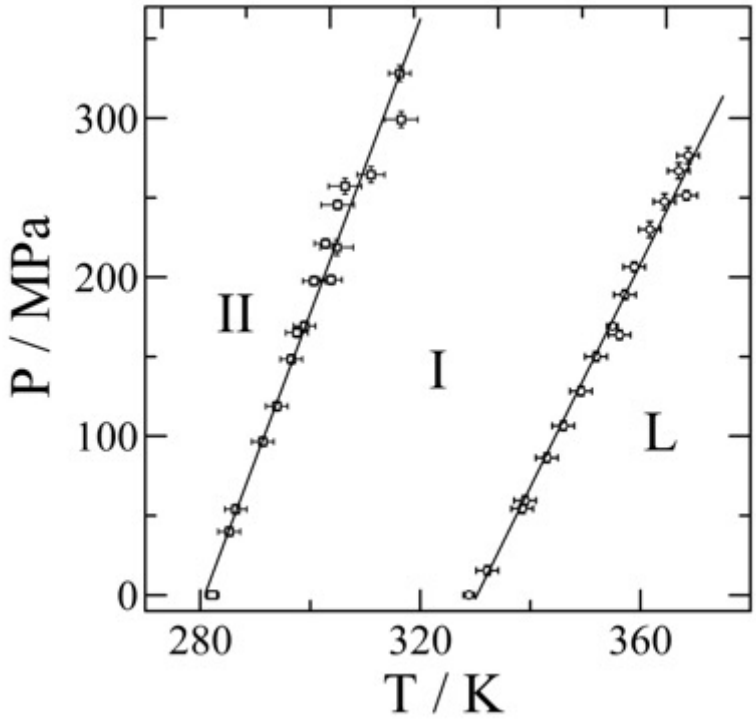

Figure 6. Pressure of the II→I (open squares) and I→L phase equilibria (open circles) as a function of the onset temperatures obtained by high-pressure differential thermal analysis. The lines are linear fits to the data (eqs. 4 and 5).

4 Discussion

4.1 Crystal structure of the low-temperature form II

Although the structure of form II has been solved at a lower temperature than that of form I, it can be seen that the two structures are very similar in their lattice parameters, in their packings (see **Figure 7**), and in their X-ray powder patterns (see **Figure 5**). Moreover, the hydrogen bonding is virtually the same in the two structures (see **Table 1**) in which atom N1 behaves as a donor through its two H-atoms and as an acceptor in a third hydrogen bond (see **Figure 8**). The hydrogen-bond patterns form centrosymmetric infinite chains parallel to the *ab* plane in both cases (see the Supporting Information **Figure S5**). Moreover, in form II as reported by Caira et al. for form I, "*the L-shaped molecular conformation allows the amino-and carbonyl- groups to engage an intermolecular bonding and the hydrophobic alkyl chains to interdigitate*".[7] The similarities of the two forms notwithstanding, a clear discontinuous change can be observed in the peak positions between 280 K (form II) and 292 K (form I), which rules out that the structures are exactly the same (See **Figure S3** in the Supporting Information).

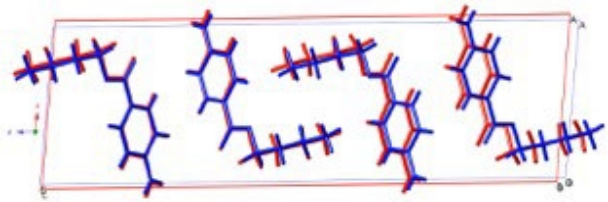

Figure 7. Packings of the butamben form I **(red)** and form II **(blue)**, both viewed along axis ***b*** with lattice parameters a = 8.3508 Å, b = 5.2093 Å, c = 25.626 Å, β = 95.372° for form I at 298 K, and a = 8.2634 Å, b = 4.7330 Å, c = 27.626 Å, β = 95.604° for form II at 120 K.

Table 1. Hydrogen bonds in the structures of polymorphs I and II of butamben

Polymorph	II	I[a]	II	I[a]	II	I[a]	II	I[a]
Bond D-H···A	d(D-H) /Å		d(H···A) /Å		d(D···A) /Å		Angle (D-H···A) /°	
N1-H6···N1	0.894	0.860	2.314	2.394	3.201	3.253	172.12	176.35
N1-H5···O1	0.868	0.860	2.029	2.113	2.876	2.950	164.75	164.32

[a] from CIF EZAVIK

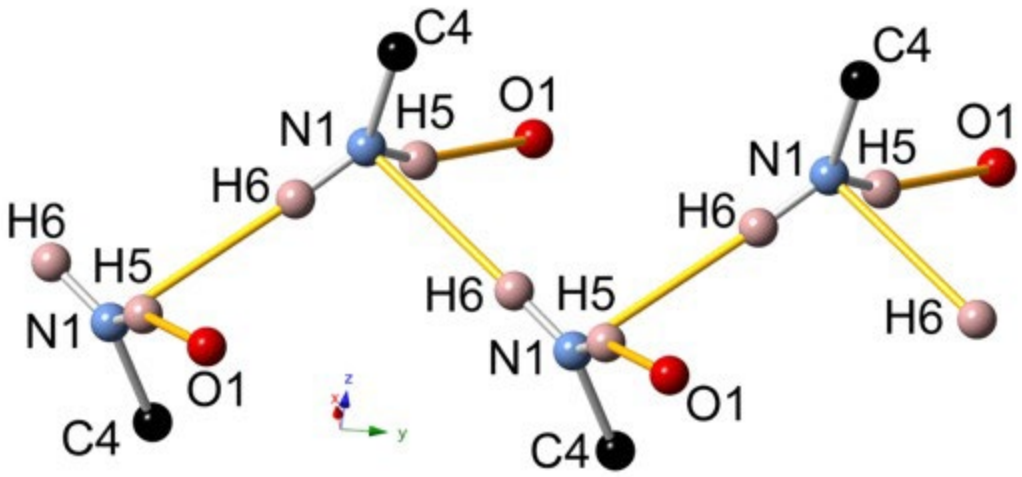

Figure 8. Detail of the hydrogen bonding pattern in butamben form II, which exhibits an infinite zig-zag chain N1···H6-N1···H6 along the b axis with lateral N1-H5···O1 bonds, while N1 is linked to aromatic carbon C4. Hydrogen bonds in yellow.

The difference in the two structures mainly consists of a small change in the orientation of the butyl chain, as shown in **Figure 9.** The two butyl-chain conformations should be very similar in energy as the values of the O-C-C-C torsion angles remain very similar (70.4° for form II at 120 K, and 73.1° for form I at RT). Therefore, the small difference in enthalpy between the two phases is probably mainly due to the slightly stronger hydrogen bonds in form II (Table 2), although the change in the torsion angles also points to a better packing and a somewhat stronger van der Waals contribution for the butyl chain.

Figure 9. The conformations of the butamben molecule in forms I (red) and II (blue). By superimposing the two phenyl rings, it can be seen that the main difference consists of a small change in the orientation of the aliphatic chain with the O-C-C-C torsion angles respectively 73.1° and 70.4°.

4.2 The melting temperature of form II at ordinary pressure

The calorimetric transition data obtained in this study and used in the analysis below are very close to those found by Svärd et al.[8] The same is true for the data obtained by Schmidt except for the enthalpy of the solid-solid transition, which is twice as large compared to the data in the present study and in that of Svärd et al.[8,20] In the following, only the mean values from **Table S3** have been used.
Because form II transforms into form I below room temperature, its melting temperature cannot be observed experimentally. Nevertheless, it can be calculated using the equation proposed by Yu[2,21] in its simplified form, i.e. neglecting the difference between the specific heats of the two polymorphs:

$$T_{II\rightarrow L} = \frac{\Delta_{II\rightarrow I}H+\Delta_{I\rightarrow L}H}{\frac{\Delta_{II\rightarrow I}H}{T_{II\rightarrow I}}+\frac{\Delta_{I\rightarrow L}H}{T_{I\rightarrow L}}} \qquad \textbf{(6)}$$

This leads to a melting temperature for form II of $T_{\mathrm{II}\rightarrow\mathrm{L}}$ = 329(16) K, while its enthalpy of fusion following Hess' law ($\Delta_{\mathrm{II}\rightarrow\mathrm{L}}H = \Delta_{\mathrm{II}\rightarrow\mathrm{I}}H + \Delta_{\mathrm{I}\rightarrow\mathrm{L}}H$) equals $\Delta_{\mathrm{II}\rightarrow\mathrm{L}}H$ = 131(5) J·g^{-1} using the values mentioned in the results section on the calorimetric data (**Table S3**).

4.3 Thermal expansion of the liquid and volume changes at $T_{I\rightarrow L}$ and $T_{II\rightarrow L}$

Using **eq. 1**, the mean expansivity of liquid butamben can be calculated with the expression $v(T) = v_0\ (1 + \alpha_v T)$ in which α_v represents the expansivity. For the liquid, it is found to be $\alpha_{v,\mathrm{L}}$ = 1.005(4) ×10^{-3} K^{-1} close to the average value of about 1.20(25) ×10^{-3} K^{-1}.[22] With **eqs. 1** to **3**, the volume changes on melting are found equal to $\Delta_{\mathrm{I\text{-}L}}v$ = 0.076 cm^3·g^{-1} and $\Delta_{\mathrm{II\text{-}L}}v$ = 0.078 cm^3·g^{-1}. These changes can also be represented as the ratio between the volume of the liquid and that of the solid leading to $v_{\mathrm{L}}/v_{\mathrm{I}}$ = 1.09 at $T_{\mathrm{I\text{-}L}}$ and $v_{\mathrm{L}}/v_{\mathrm{II}}$ =1.09 at $T_{\mathrm{II\text{-}L}}$. These two values are somewhat smaller, but nonetheless quite close to the average increase in specific volume on melting of 11% for small organic molecules including APIs.[22-24]

4.4 Thermal expansion of forms I and II and the volume change at $T_{II\rightarrow I}$

It can be seen in **Supporting information** **Figure S6** that on heating, the II→I phase transition is accompanied with an increase in the unit-cell parameters *a* and *b* and a decrease in the unit-cell parameter *c* and the angle β (see also the polynomial fits of the

unit-cell parameters in **Table S7**). It can be seen in **Figure 10** that these changes give rise to a very small increase in the specific volume at the temperature at which the II-I equilibrium shifts. With **eqs. 2** and **3**, the volume change at the transition temperature $T_{II \rightarrow I}$ = 282.9 K is found to be $\Delta_{II \rightarrow I}v$ = 0.0006 cm^3·g^{-1}, a very small positive value.

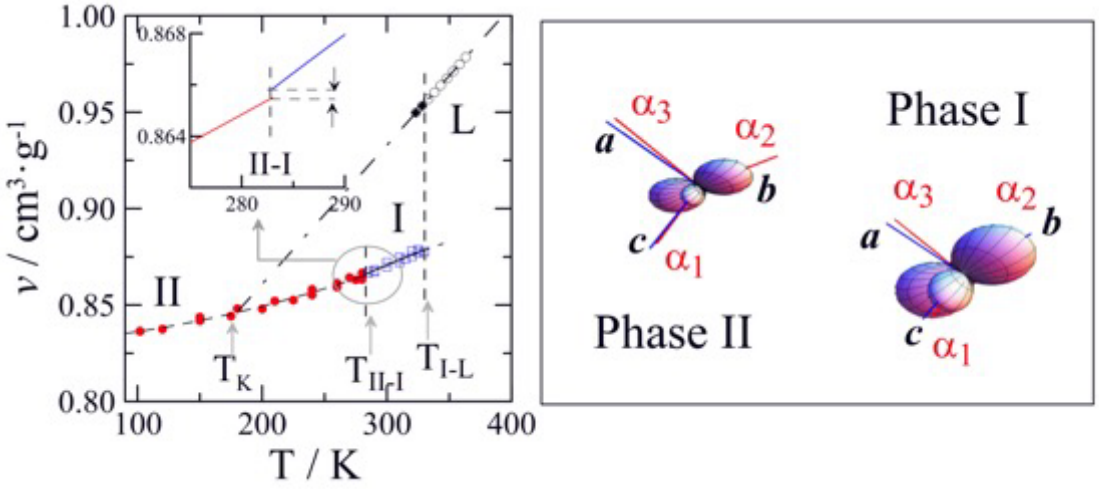

Figure 10. **Left-hand panel:** specific volume of form II (filled red circles) and form I (open blue squares) and the liquid (black circles) as a function of temperature with T_k the Kauzmann temperature. Filled black circles correspond to the supercooled liquid phase. **Inset:** close-up of the positive volume change of the II→I transition. **Right-hand panel:** graphic representation of the thermal expansion tensor of form I (bottom-right) at 300 K and form II (top-left) at 250 K.

For the mean expansivity of form I, $\alpha_{v,I}$, a value of 3.40 ×10^{-4} K^{-1} is found with **eq. 2**. In the case of form II, the quadratic equation **eq. 3** needs to be approximated by a linear equation:

$$v_{II}\ /\text{cm}^3\cdot\text{g}^{-1} = 0.8183(14) + 1.62(7) \times 10^{-4}\ T\ /\text{K} \qquad (r^2 = 0.97) \qquad (3')$$

The mean expansivity with **eq. 3'** becomes $\alpha_{v,II}$ = 1.98(9) × 10^{-4} K^{-1}, which virtually matches the average value of 2 ×10^{-4} K^{-1} for the expansivities reported for solids of organic compounds in general[25] and for pharmaceuticals.[22,23,26-30] The expansivity of form I, obtained from eq. 2 ($\alpha_{v,L}$ = 3.4(3) × 10^{-4} K^{-1}), is considerably larger than this average and the expansivity of form II, which is most likely caused by the small temperature range at which the expansion has been determined in addition to the fact that this range lies close to the melting point of form I.

In order to account for the anisotropy of the intermolecular interactions, the second-rank thermal-expansion tensor has been calculated from the lattice parameters as a function of temperature for phases I and II. Owing to the monoclinic symmetry of both phases, thermal-expansion tensors are defined by the orthonormal principal coefficients (α_1, α_2, α_3) with the α_2 eigenvector being parallel to the two-fold unit-cell axis ***b***. The eigenvalues as a function of temperature have been compiled in the Supporting information **Table S8**. The 3D thermal-expansion tensor is represented in **Figure 10** at 250 K for phase II and at 300 K for phase I. The overall expansivity α_v, as discussed above, is higher in the high-temperature phase I. In **Figure 10** (as well as in **Table S8** in the Supporting information) the existence of negative eigenvalues (α_1) can be observed close to the crystallographic ***c***

axis together with small values in α_3 (close to the ***a*** axis), whereas the maximum deformation of the cell can be observed in the α_2 direction, parallel to the ***b*** two-fold crystallographic axis. It implies that the α_2 direction (i.e. along ***b***) is the soft direction, while the ***ac*** plane (containing the α_1 and α_3 eigenvectors) is a hard plane for both phases I and II.[31] In both phases, the hard plane contains the centrosymmetric infinite hydrogen bonded chains and the interlocked butyl chains (see **Figure S5**), while in the ***b*** direction the stacking mainly depends on van der Waals interactions and zigzag hydrogen-bond chains that have some flexibility in their displacement.

4.5 Topological Pressure-Temperature diagram involving the condensed phases

Two-phase equilibrium curves in the pressure-temperature space involving two polymorphs or a crystalline solid and its liquid can be described over a considerable range of pressures by a straight line. The slopes of these equilibria, dP/dT, can be calculated with the Clapeyron equation:

$$\frac{dP}{dT} = \frac{\Delta S}{\Delta v} = \frac{\Delta H}{T\Delta v} \qquad (7),$$

if the temperatures, enthalpy changes, and volume changes are known for the phase transformations at ordinary pressure.

For equilibrium I-II, with values $T_{II\rightarrow I}$ = 282.9 K, $\Delta_{II\rightarrow I}H$ = 1.94(50) J·g^{-1}, and $\Delta_{II\rightarrow I}v$ = 0.0006 cm^3·g^{-1}, it is found that $dP/dT_{II\rightarrow I}$ = 11 MPa·K^{-1}.
For equilibrium I-L, with values $T_{I\rightarrow L}$ = 330.2 K, $\Delta_{I\rightarrow L}H$ = 128.7(4.4) J·g^{-1}, and $\Delta_{I\rightarrow L}v$ = 0.076 cm^3·g^{-1}, it is found that $dP/dT_{I\rightarrow L}$ = 5.1(7) MPa·K^{-1}.

The purpose of the topological method is to identify to which of the four cases of dimorphism, established by Bakhuis-Roozeboom,[3,5] the case under study belongs to and not necessarily to provide a highly accurate pressure-temperature phase diagram. Concerning the dimorphism of butamben, it belongs to case 2, overall enantiotropy, because the slope of the I-II equilibrium line is much steeper than the slope of the I-L equilibrium curve, thus indicating that the two curves diverge on increasing pressure. This implies that the II-L equilibrium curve, the melting of form II, must also diverge in relation to both curves with increasing pressure.

4.6 Experimental phase diagram involving the condensed phases

The high-pressure data shown in **Figure 6** unambiguously confirm that the dimorphism of butamben corresponds to a case of overall enantiotropic behaviour.[3,5] The two equilibrium curves of I-II and I-L diverge as the pressure increases so that each polymorph exhibits its own stable phase region regardless of the pressure. The phase diagram can be improved by locating the other equilibrium curves together with the triple points leading to a complete topological representation of the phase diagram, as described in the following section.

4.6.1 Location of the triple points

4.6.1.1 Triple point I-II-L

The I-II-L triple point is the intersection of the I-II and I-L experimental equilibrium curves. By setting eqs. 4 and 5 equal to each other, the triple point coordinates can be estimated as: $T_{\text{I-II-L}}$ = 124(15) K, $P_{\text{I-II-L}}$ = −1448(282) MPa. Such a triple point is metastable because it occurs at negative pressure implying that the system is in an expanded state.

The I-II-L triple point can be used to place the II-L equilibrium in the phase diagram. The melting point of form II has been calculated above using the Clapeyron equation (**eq. 7**). This melting point is in itself also a triple point, or at least its temperature will be very close to the triple point II-L-V, V being the vapour in equilibrium with the solid and the liquid at fusion. Thus, the II-L-V triple point possesses the coordinates: T = 329.4 K, P = 0 MPa. Because the II-L curve, taken as a straight line passes through triple points II-L-V and I-II-L whose coordinates were calculated above, the equation for the II-L equilibrium is found to be:

$$P_{\text{II-L}}\,/\text{MPa} = -2322 + 7.1\,T\,/\text{K} \qquad (8).$$

4.6.1.2 Triple points involving the vapor phase

In the same way as triple point II-L-V has been determined, the triple points I-II-V and I-L-V can be defined too. The temperatures of the II→I transition and of the fusion of form I have been determined by DSC experiments. During these experiments the dead volume in the capsules will be filled by the vapor of butamben, which may bring it close to the equilibrium vapor. In any case, even out of equilibrium, the difference between the triple point temperature and the transition temperature obtained by DSC may differ less than the actual measurement error and can thus be set equal.

Once the triple points involving the vapour phase have been established, the equilibrium vapour pressure can be calculated with the following approach. The boiling point of butamben has been predicted by ACD/Labs PhysChem Suite[32] to be 325.68 °C ($T_{\text{L}\rightarrow\text{V}}$ = 598.83 K) together with an enthalpy of vaporization $\Delta_{\text{L}\rightarrow\text{V}}H$ of 56.782 kJ·mol^{-1} (or 293.84 J·g^{-1}). Using these values, the vaporization curve in the pressure-temperature phase diagram can be described by a Clausius-Clapeyron type equation:

$$\ln(P_{\text{V}}) = -\Delta_{\text{L}\rightarrow\text{V}}H/(RT) + B_{\text{L}\rightarrow\text{V}} \qquad (9)$$

in which P_{V} is the vapor pressure in Pa and $\Delta_{\text{L}\rightarrow\text{V}}H$ is the enthalpy change of vaporization in J·mol^{-1} with R, the gas constant, equal to 8.3145 J·mol^{-1}·K^{-1}, and P_{V} = 1.0133 ×10^{5} Pa at the boiling temperature. Using this information, the constant $B_{\text{L}\rightarrow\text{V}}$ is found to be equal to 22.93. Introducing this value in **eq. 9** together with $T_{\text{I-L}}$ = 330.2 K, i.e. the temperature of the I-liquid-vapor triple point, the vapor pressure at this triple point is found to be 9.5 Pa. At a triple point involving two condensed phases in equilibrium, the vapour pressure of both phases must be the same. According to Hess' law, the sublimation enthalpy is the algebraic sum of the melting and vaporization enthalpies ($\Delta_{\text{sub}}H = \Delta_{\text{fus}}H + \Delta_{\text{vap}}H$), the P-T sublimation curves of forms I and II can be determined by repeating the approach with the vaporization curve.
Thus, at the melting point of form I, $T_{\text{I-L-V}}$ = 330.2 K, the pressure is known to be 9.5 Pa and the enthalpy of sublimation of form I is $\Delta_{\text{I}\rightarrow\text{V}}H = \Delta_{\text{I}\rightarrow\text{L}}H + \Delta_{\text{L}\rightarrow\text{V}}H$ = 81.655 kJ·mol^{-1}. With the

Clausius Clapeyron equation (eq. 8), this leads to a value for $B_{I\rightarrow V}$ of 31.99. For form II, the vapour pressure at the II-L-V can be calculated with the vapour pressure curve for the liquid, which leads to $P_{II\text{-}L\text{-}V}$ = 9.0 Pa. Using the sublimation enthalpy of form II, $\Delta_{II\rightarrow V}H = \Delta_{II\rightarrow L}H + \Delta_{L\rightarrow V}H$, which equals 82.030 kJ·mol^{-1} and the triple point temperature $T_{II\text{-}L\text{-}V}$ = 329.4 K, $B_{II\rightarrow V}$ is found to be 32.15.
Setting the Clausius–Clapeyron equations describing the sublimation curves of forms I and II equal, results once again in $T_{I\text{-}II\text{-}V}$ = 282.9 K (because this approach is equivalent to eq. 6) and the value of the sublimation pressure at the triple point I-II-V is found to be $P_{I\text{-}II\text{-}V}$ = 6.6 ×10^{-2} Pa. Thus, in conclusion of this section, the coordinates of triple points involving the vapour phase are:
I-L-V: $P_{I\text{-}L\text{-}V}$ = 9.5 Pa, $T_{I\text{-}L\text{-}V}$ = 330.2 K
II-L-V: $P_{II\text{-}L\text{-}V}$ = 9.0 Pa, $T_{II\text{-}L\text{-}V}$ = 329.4 K
I-II-V: $P_{I\text{-}II\text{-}V}$ = 6.6 × 10^{-2} Pa, $T_{I\text{-}II\text{-}V}$ = 282.9 K.
Although the pressure values are negligible in terms of the pressure coordinate in MPa in the topological phase diagram, they do demonstrate the consistency in the thermodynamic ranking of the phases and the phase transitions.

5 Concluding remarks

The structures of forms I and II strongly resemble each other with virtually no difference in their packings. They both contain infinite chains of hydrogen bonds within the ***ac*** monoclinic plane. The similarity of the polymorphic structures and the small difference in enthalpy make it hard to point out the cause of the change in the stability hierarchy between the two solid phases, not in the least, because the enthalpy difference is clearly within the error of the energy differences that computer-aided energy calculations can provide even if experimentally the change in enthalpy can be observed (cf. **Figure 3** and **Table S3** in the supporting information).

This does not imply that the phase transition does not exist, however. Although the geometries of the molecules are very similar, it is clear that as a function of temperature a reversible volume change occurs at about 283 K. The discontinuity in the specific volume is accompanied by a discontinuity in the specific enthalpy (observed by DSC and by high-pressure DTA) and combined these discontinuities are the classic thermodynamic signature of a first-order phase transition. Such a transition is, according to the Ehrenfest classification,[33,34] characterized by "*a jump in the first-order derivatives of the Gibbs energy, ΔS and ΔV*".[35,36] Similar and even more unusual cases can be found in the literature. For example, Coles et al. found the same packing in two polymorphs of 3-chloromandelic acid, and they named them "isostructural polymorphs".[37] On a more mundane level are polymorphs with small orientational differences in the aliphatic chain that clearly demonstrate discontinuities in specific volume and enthalpy; examples of these cases are chlorpropamide,[38-41] and tolazamide.[42]

A complete topological pressure-temperature phase diagram of the dimorphism of butamben with four triple points is provided in **Figure 11**. It is an example of an overall enantiotropic system. It demonstrates once more that with the Clapeyron equation, data obtained at ordinary pressure can be used to construct a realistic topological pressure-temperature phase diagram and to determine the overall phase behaviour in terms of the four cases of dimorphism described by Bakhuis Roozeboom. Similar phase diagrams can

also be found in some recently studied cases: benzylthiouracil,[43] trinitrotoluene,[44] and nimesulide.[45]
For butamben, the experimental and calculated slopes of the two-phase equilibrium curves are numerically not exactly the same: 9.24 and 7.02 MPa·K^{-1} for the experimental dP/dT values of the I-II and I-L equilibria, against 11 and 5.14 MPa·K^{-1} for the calculated (eq. 7) ones, respectively. However, both results clearly lead to the same topological conclusion of overall enantiotropy. It can be concluded that at room temperature, form I remains stable up to at least 120 MPa. In addition, because the I-II equilibrium curve is quite steep, it can be inferred that the shift of the equilibrium from form II to form I (with a small volume change) hardly depends on the pressure. Because it shifts right on increasing the temperature, it can be concluded that the transition is mainly entropy-driven, even if the enthalpy change is rather small for such a transition.

The volume change on melting corresponds to a ratio $v_{\text{liquid}}/v_{\text{solid}}$ of 1.09 for the two forms, i.e. close to the average value of 1.11 previously inferred from data involving 10 active pharmaceutical ingredients.[27] It is also close to the conclusion of Goodman et al., who reported "*a ratio of solid to liquid density at the triple point of 1.12... with an estimated average uncertainty of about 6%*" (i.e., 1,12(7))".[46] Whether this ratio approaches a constant value, as previously questioned[27] remains to be answered through more experimental work.

From a pharmaceutical perspective, a reversible phase change at 283 K (10°C) is rather problematic as during storage and transportation the surroundings of the drugs may easily pass through this temperature multiple times causing sudden increases and decreases of the crystal volume resulting in mechanical stresses in the formulation. This may cause disintegration of the crystals and of the tablets that contain the drug. In the case of butamben, the volume change may be small, but it remains a point of concern that will need to be kept in mind.
The pressure dependency of the phase transition could also be problematic in the case of tabletting. In the present case the slope of the I-II equilibrium is rather steep. The experimental slope of 9.24 MPa·K^{-1} indicates that for each degree of warming, the pressure of the equilibrium increases with 9 MPa. Thus, if the phase transition occurs at 10°C under ordinary conditions, at 20°C the equilibrium will be at 90 MPa and at 30°C at 180 MPa. These numbers are clearly still in the working zone of tabletting and although the equilibrium is easily reversible, it may cause the tabletting to be much less effective. One remedy for butamben, based on its phase diagram, would be to carry out tabletting at higher temperatures avoiding the phase equilibrium.

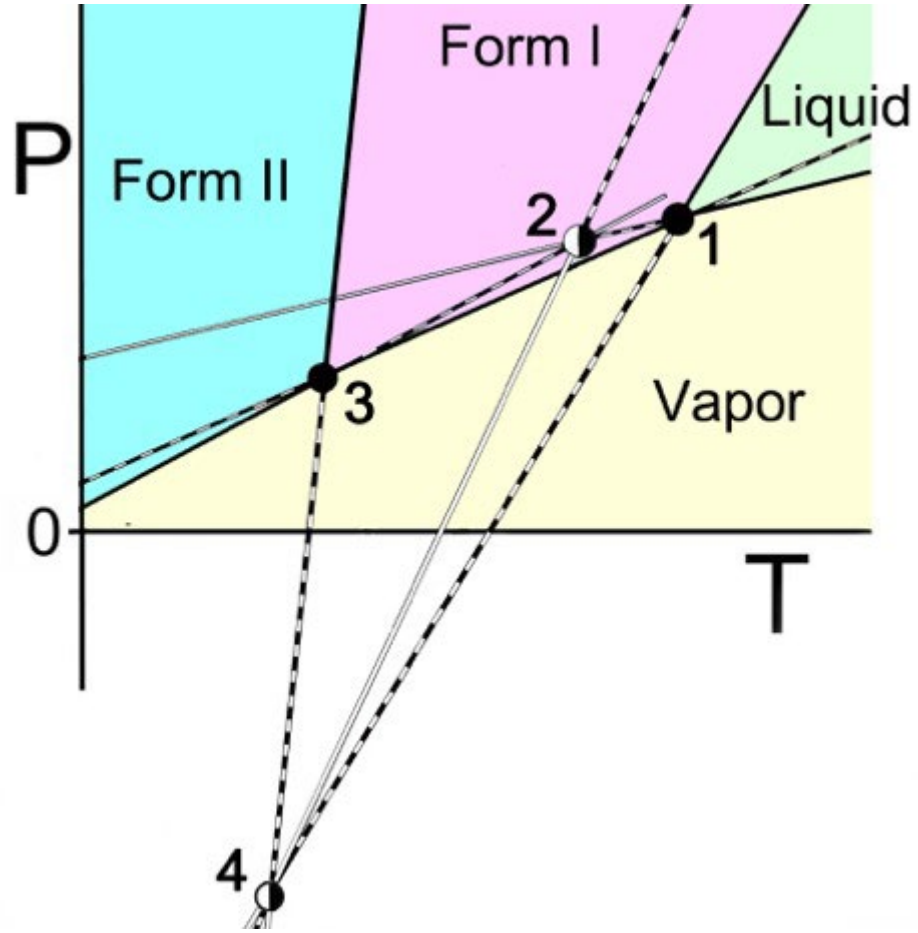

Figure 11. Topological pressure-temperature phase diagram for the dimorphism of butamben. Stable (filles circles) and metastable (half-filled circles) triple points: **1** = I-liquid-vapor, **2** = II-liquid vapor, **3** = I-II-vapor, **4** = I-II-liquid. Two-phase equilibrium lines: **1-2** = liquid-vapor, **1-4** = I-liquid, **2-4** = II-liquid, **3-4** = I-II, **1-3** = I-vapor, **2-3** = II-vapor. Black lines = stable, dashed lines = metastable, open lines = super-metastable phase equilibria.

Acknowledgements
This work was supported by MINECO Project No. FIS2017-82625- P and AGAUR DGU Project No. 2017SGR-42.

Declaration of Competing Interest
The authors declare no competing interest.

Supporting Information
Table S1. Crystal data and structure refinement for butamben form II, **Table S2.** Atom coordinates of the low-temperature form II of butamben, **Table S3.** Onset temperatures and heats of transition at various heating rates, **Table S4.** Density and the specific volume of molten butamben as a function of temperature, **Table S5.** Lattice parameters and specific volumes for forms I and II as a function of temperature, **Table S6.** Pressure values at the onset temperatures of the butamben phase transitions, **Table S7.** Polynomial fits of the unit-cell parameters for forms I and II, **Table S8.** The eigenvalues of the thermal expansion tensor, **Figure S1.** Molecular structure and conformation in the low-temperature form II, **Figure S2.** A full PXRD pattern of butamben **Figure S3.** 2θ values of the Bragg peaks indicated in **Figure 5**, **Figure S4.** Butamben high-pressure differential

thermal analysis: Typical peaks recorded at various pressures, **Figure S5.** Centrosymmetric infinite chains of butamben form II parallel to the *y* axis, **Figure S6.** Lattice parameters versus temperature demonstrating the first-order phase change.

References

(1) Schmidt, A. C., *Int. J. Pharm.* **2005,** 298, 186-197.
(2) Gana, I.; Barrio, M.; Do, B.; Tamarit, J.-L.; Céolin, R.; Rietveld, I. B., *Int. J. Pharm.* **2013,** 456, 480-488.
(3) Bakhuis Roozeboom, H. W., *Die heterogenen Gleichgewichte vom Standpunkte der Phasenlehre. Erstes Heft: Die Phasenlehre - Systeme aus einer Komponente.* ed.; Friedrich Vieweg und Sohn: Braunschweig, 1901; Vol. 1.
(4) Ceolin, R.; Tamarit, J. L.; Barrio, M.; Lopez, D. O.; Nicolai, B.; Veglio, N.; Perrin, M. A.; Espeau, P., *J. Pharm. Sci.* **2008,** 97, 3927-41.
(5) Ceolin, R.; Rietveld, I.-B., *Ann. Pharm. Fr.* **2016,** 74, 12-20.
(6) Watanabe, A., *Yakugaku Zasshi* **2002,** 122, 595-606.
(7) Caira, M. R.; Bourne, S. A.; Vilakazi, S. L.; Reddy, L., *Supramol. Chem.* **2004,** 16, 279-285.
(8) Svärd, M.; Zeng, L.; Valavi, M.; Krishna, G. R.; Rasmuson, Å. C., *J. Pharm. Sci.* **2019,** 108, 2377-2382.
(9) Rodriguez-Carvajal, J., *Physica B* **1993,** 192, 55-69.
(10) Rodriguez-Carvajal, J.; Roisnel, T.; Gonzales-Platas, J. *Full-Prof suite version 2005*, Laboratoire Léon Brillouin, CEA-CNRS, CEN Saclay, France, 2005.
(11) Würflinger, A., *Ber. Bunsen-Ges. Phys. Chem.* **1975,** 79, 1195-1201.
(12) Aznar, A.; Lloveras, P.; Kim, J. Y.; Stern-Taulats, E.; Barrio, M.; Tamarit, J. L.; Sanchez-Valdes, C. F.; Sanchez Llamazares, J. L.; Mathur, N. D.; Moya, X., *Adv Mater* **2019,** 31, e1903577.
(13) Finger, L. W.; Cox, D. E.; Jephcoat, A. P., *J. Appl. Crystallogr.* **1994,** 27, 892-900.
(14) Thompson, P.; Cox, D. E.; Hastings, J. B., *J. Appl. Crystallogr.* **1987,** 20, 79-83.
(15) Boultif, A.; Louër, D., *J. Appl. Crystallogr.* **1991,** 24, 987-993.
(16) Markvardsen, A. J.; David, W. I. F.; Johnson, J. C.; Shankland, K., *Acta Crystallogr. A* **2001,** 57, 47-54.
(17) Coelho, A. A. *TOPAS Academic version 4.1 (Computer Software)*, Coelho Software: Brisbane, 2007.
(18) Dollase, W. A., *J. Appl. Crystallogr.* **1986,** 19, 267-272.
(19) Bruno, I. J.; Cole, J. C.; Kessler, M.; Jie, L.; Motherwell, W. D. S.; Purkis, L. H.; Smith, B. R.; Taylor, R.; Cooper, R. I.; Harris, S. E.; Orpen, A. G., *J. Chem. Inf. Comput. Sci.* **2004,** 44, 2133-2144.
(20) Schmidt, A. C., *Int. J. Pharm.* **2005,** 298, 186-197.
(21) Yu, L., *J. Pharm. Sci.* **1995,** 84, 966-974.
(22) Céolin, R.; Rietveld, I. B., *Ann. Pharm. Fr.* **2015,** 73, 22-30.
(23) Rietveld, I. B.; Céolin, R., *J. Therm. Anal. Calorim.* **2015,** 120, 1079-1087.
(24) Ceolin, R.; Rietveld, I. B., *Ann. Pharm. Fr.* **2017,** 75, 89-94.
(25) Gavezzotti, A., *Molecular Aggregation. Structure Analysis and Molecular Simulation of Crystals and Liquids*. ed.; Oxford University Press: Oxford, UK, 2013; p 448.
(26) Li, K.; Gbabode, G.; Barrio, M.; Tamarit, J.-L.; Vergé-Depré, M.; Robert, B.; Rietveld, I. B., *Int. J. Pharm.* **2020,** 580, 119230.

(27) Rietveld, I. B.; Negrier, P.; Barrio, M.; Allouchi, H.; Ceolin, R.; Tamarit, J. L., *Int. J. Pharm.* **2021,** 593, 120124.
(28) Allouchi, H.; Nicolai, B.; Barrio, M.; Ceolin, R.; Mahe, N.; Tamarit, J.-L.; Do, B.; Rietveld, I. B., *Cryst. Growth Des.* **2014,** 14, 1279-1286.
(29) Mahe, N.; Nicolai, B.; Barrio, M.; Perrin, M.-A.; Do, B.; Tamarit, J.-L.; Ceolin, R.; Rietveld, I. B., *Cryst. Growth Des.* **2013,** 13, 3028-3035.
(30) Mahé, N.; Nicolaï, B.; Allouchi, H.; Barrio, M.; Do, B.; Céolin, R.; Tamarit, J.-L.; Rietveld, I. B., *Cryst. Growth Des.* **2013,** 13, 708-715.
(31) Salud, J.; Barrio, M.; Lopez, D. O.; Tamarit, J. L.; Alcobe, X., *J. Appl. Crystallogr.* **1998,** 31, 748-757.
(32) ACD/Labs *ACD/Labs*, version 12; Advanced Chemistry Development, Inc.: Toronto, Ontario, Canada.
(33) Jaeger, G., *Arch. Hist. Exact Sci.* **1998,** 53, 51-81.
(34) Ehrenfest, P., *Verhandlingen der Koninklijke Akademie van Wetenschappen* **1933,** 36, 153-157.
(35) Hillert, M., *Phase Equilibria, Phase Diagrams and Phase Transformations, Their Thermodynamic Basis*. 2nd ed. ed.; Cambridge University Press: Cambridge UK, 2008.
(36) Cuevas-Diarte, M. A.; Oonk, H. A. J., *Molecular Mixed Crystals*. Springer: Cham, 2021; p 44.
(37) Coles, S. J.; Threlfall, T. L.; Tizzard, G. J., *Cryst. Growth Des.* **2014,** 14, 1623-1628.
(38) Drebushchak, T. N.; Chukanov, N. V.; Boldyreva, E. V., *Acta Crystallogr. C* **2007,** 63, o355-7.
(39) Drebushchak, T. N.; Chesalov, Y. A.; Boldyreva, E. V., *Acta Crystallogr B* **2009,** 65, 770-81.
(40) Drebushchak, T. N.; Drebushchak, V. A.; Boldyreva, E. V., *Acta Crystallogr B* **2011,** 67, 163-76.
(41) Zakharov, B. A.; Goryainov, S. V.; Boldyreva, E. V., *CrystEngComm* **2016,** 18, 5423-5428.
(42) Boldyreva, E. V.; Arkhipov, S. G.; Drebushchak, T. N.; Drebushchak, V. A.; Losev, E. A.; Matvienko, A. A.; Minkov, V. S.; Rychkov, D. A.; Seryotkin, Y. V.; Stare, J.; Zakharov, B. A., *Chemistry* **2015,** 21, 15395-404.
(43) Rietveld, I. B.; Allouchi, H.; Barrio, M.; Ceolin, R.; Tamarit, J. L., *Int. J. Pharm.* **2021,** 598, 120378.
(44) Céolin, R.; Rietveld, I. B., *Fluid Phase Equilib.* **2020,** 506, 112395-112400.
(45) Barrio, M.; Huguet, J.; Robert, B.; Rietveld, I. B.; Ceolin, R.; Tamarit, J. L., *Int. J. Pharm.* **2017,** 525, 54-59.
(46) Goodman, B. T.; Wilding, W. V.; Oscarson, J. L.; Rowley, R. L., *J. Chem. Eng. Data* **2004,** 49, 1512-1514.